



Characterising airflow and heat transfer within a multi-package of horticultural produce using a validated CFD model

Ahmad Nasser eddine^{a,*}, Steven Duret^a, Denis Flick^b, Jean Moureh^a

^a INRAE, FRISE, Université Paris-Saclay, Antony 92761, France

^b INRAE, AgroParisTech, UMR SayFood, Université Paris-Saclay, Palaiseau 91120, France

ARTICLE INFO

Keywords:

Modified Atmosphere Package
Multi-package
Airflow behaviour
Cooling behaviour
Computational fluid dynamics

ABSTRACT

Modified Atmosphere Packaging (MAP) is extensively used for highly perishable items to extend their shelf life by reducing their physiological activity. However, this solution involves non-ventilated packaging materials which hinder direct contact of cooling air with the product, thereby affecting the cooling rate of MAPs when packaged in ventilated trays. This research developed a Computational Fluid Dynamics (CFD) model to predict airflow within a half layer of a strawberry-ventilated pallet, consisting of two trays with 16 airtight clamshells (AC) each, representing modified atmosphere packaging. Within the ACs, the internal domain was modelled as an equivalent solid block representing both air and strawberries. Three tray designs were compared to assess the impact of vent holes and their positions on airflow behaviour and cooling rate. The model was validated using experimental data, showing a good agreement for air velocities and cooling characteristics.

The analysis revealed that in the current tray design (TD 1) with a single main trapezoidal orifice on the longitudinal surface, airflow was uneven, with 24 % traversing the headspace and 76 % through the channels between ACs. This design caused recirculation near the tray's edge and poor ventilation within the channels of this area, leading to heterogeneous cooling among ACs. This heterogeneity in cooling resulted in differences of up to 2 h in Half Cooling Time. Numerical simulations indicated that adding vent holes to the tray does not guarantee an improved cooling rate and uniformity. The effectiveness of vent holes depended on their placement relative to ACs arrangement.

1. Introduction

Cold chain operations play a vital role in minimizing postharvest losses. The critical initial step in this process: precooling, involves removing field heat to bring the horticultural product's temperature down to an optimal level. Subsequent logistic operations focus on maintaining this temperature, thus preventing any abuse. These steps are instrumental in mitigating various biological, biochemical, and microbiological phenomena like transpiration, respiration, ripening, and spoilage. The overarching goal of these operations is to preserve the natural characteristics of the product, including its appearance, texture, and flavour, throughout the postharvest period up to the point of consumption (Dehghannya et al., 2011). However, disruptions or mismanagement in the cooling process can result in uneven or inconsistent cooling, potentially causing product deterioration. These issues can stem from a range of factors, including the operating conditions and the design of the packaging. Notably, packaging design significantly impacts

cooling efficiency, directly affecting product quality (Pathare et al., 2012).

Both experimental and numerical studies focusing on airflow, heat, and mass transfer are essential for understanding how packaging design, product arrangement, and multi-package systems impact airflow, as well as the interaction between cooling and airflow.

While experimental studies provide realistic insights considering the variability in products and operating conditions, they are often costly and time-consuming (Nasser Eddine et al., 2022), and particularly difficult when dealing with biological materials (Delele et al., 2013b). Velocity and temperature measurements are the two essential parameters measured when conducting experiments (Alvarez and Flick, 1999a; 1999b; Anderson et al., 2004; Duret et al., 2014; Pham et al., 2019a; 2019b; Wu et al., 2018).

While the multi-packaging system offers significant benefits in safeguarding perishable horticultural products from mechanical damage and contamination (Ngcobo et al., 2013) it also impacts airflow by

* Corresponding author.

E-mail address: ahmad.nasser-eddine@inrae.fr (A. Nasser eddine).

limiting its passage through the packaging and increasing the pressure drop (Berry et al., 2015). This creates a barrier between the product and the cooling air, necessitating an adequate cooling approach to ensure the products are effectively preserved, particularly when the primary packaging is not ventilated as a modified atmosphere packaging (MAP). However, analysing such systems is challenging due to the complexity of the interaction between the cooling air around the MAPs and the produce inside the MAP. Therefore, the product temperature evolution is highly dependent on the convective heat transfer coefficient (CHTC) on the packaging walls of MAPs.

Computational Fluid Dynamics (CFD) is well recognized in the study of cold chain logistics for fresh produce, as a time-efficient alternative to experimental methods (Nasser Eddine et al., 2022). CFD, utilizing digital computers and solving Navier-Stokes equations, simplifies the analysis by assuming similar conditions for all products, thus providing a more idealized scenario (Ambaw et al., 2021). This approach is effective for predicting airflow and temperature patterns in fruit stacks under different systems and operating conditions (Dehghannya et al., 2010; Mukama et al., 2020).

The enhancements in computational capabilities and the sophistication of CFD software have significantly improved the reliability and precision of these simulations. This progress has facilitated a more intricate understanding of the complex fluid dynamics within packaging systems for agricultural produce (Zhao et al., 2016). Researchers have developed various CFD models to study airflow in packaging and evaluate the performance of different packaging design (Agyeman et al., 2023; Delele et al., 2013a; Gruyters et al., 2019; Hoang et al., 2015; Nalbandi and Seiedlou, 2020; Wang et al., 2020).

Ferrua and Singh (2009) developed a CFD model to characterise the heat transfer and airflow behaviour within a tray filled with ventilated plastic clamshells containing strawberries during precooling, revealing cooling heterogeneity between the clamshells along the airflow direction.

However, no studies have focused on characterising the airflow patterns within multi-packaging system, including non-ventilated clamshells (MAPs). To address this gap, the present study developed a CFD model to better understand the airflow dynamics within strawberries multi-packaging system, where non-ventilated clamshells (airtight clamshells, ACs) act as the primary packaging and trays as the secondary packaging during precooling. The impact of this behaviour on cooling rates and heterogeneity was also assessed. The simulation results were validated against experimental data related to velocity levels around ACs and cooling characteristics (i.e. Half Cooling Time: HCT and Seven Eight Cooling Time: SECT). The validated model was used to assess the effect of adding circular orifices, along with their position in the tray, on the uniformity of airflow behaviour and, subsequently, the cooling rate.

2. Materials and methods

The standard industry setup for strawberry pallets typically consists

of several layers, with each layer holding four corrugated trays. In this study, considering the symmetrical layout of the trays on each pallet layer and to simulate the forced air precooling process, only half of a pallet layer was examined, corresponding to two trays. Detailed dimensions of the tray and AC used are depicted in Fig. 1a and b.

2.1. Experimental study

In this research, the experimental device designed by Nasser eddine et al. (2023) was used and conducted within a controlled environment. Airtight clamshells were used, each containing 20 PVC strawberries. The main feature of the AC's design is the integrated edge used to seal the top film. The strawberries were filled with a carrageenan gel mixture, chosen for its thermal properties, specifically thermal conductivity and specific heat capacity, that closely approximate those of real strawberries, as detailed in Table 1. This approach successfully mitigated food wastage concerns and facilitated the work with perishable food like strawberries while avoiding the drawbacks of fruit variability in terms of size and ripening.

The fans were regulated to have an airflow rate equal to 8.9 l s^{-1} which is representative of forced air precooling.

2.2. Temperature measurements

Reflecting the symmetric configuration of the airtight clamshells (AC) within a tray, temperature measurements were conducted on one half of the tray to evaluate the cooling dynamics. Temperature readings were taken from five strawberries situated at positions AC 1-2-7-8-9-10-15-16 (as indicated in blue in Fig. 2). In total, the temperatures of 40 strawberries were monitored at 10 s intervals using T-type calibrated thermocouples with a precision of $\pm 0.1 \text{ K}$. These measurements were recorded through a data logger (Keysight DAQ970A) and processed using acquisition software (Keysight BenchVue).

To standardize the initial conditions, the cold room was initially set to $20 \text{ }^\circ\text{C}$, ensuring uniform temperatures across all products. The setup was then insulated with polystyrene foam, and the device's fans were turned off to halt air circulation. Subsequently, the temperature in the cold room was lowered to $4 \text{ }^\circ\text{C}$. After a 30 min period for temperature stabilization at $4 \text{ }^\circ\text{C}$, the polystyrene foam was removed from the inlet and outlet of the setup, and the fans were activated to start the cooling experiment. The experiment was repeated twice, and for each

Table 1

Thermophysical properties of real strawberries and carrageenan gel.

Properties	Strawberries (Wang et al., 2019)	Carrageenan Gel (Agyeman et al., 2023)
$\lambda \text{ (W}\cdot\text{m}^{-1}\cdot\text{K}^{-1}\text{)}$	0.56	0.52
$\rho \text{ (kg}\cdot\text{m}^{-3}\text{)}$	800	1013
$C_p \text{ (J}\cdot\text{kg}^{-1}\cdot\text{K}^{-1}\text{)}$	4000	4100

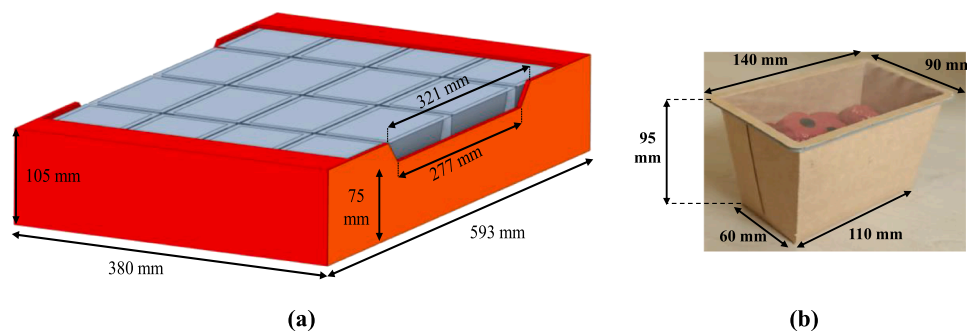


Fig. 1. (a) Tray dimensions, (b) AC dimensions.

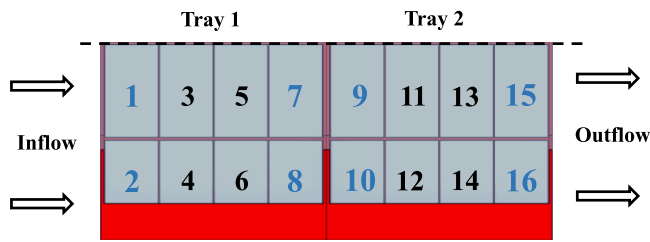


Fig. 2. Position of instrumented ACs with thermocouples.

strawberry in each AC, the half-cooling time (HCT) and seven-eighths cooling time (SECT) were calculated. The maximum standard deviations obtained were 0.04 h for HCT and 0.21 h for SECT respectively.

2.3. Velocity measurements

Air velocity measurements inside the trays were conducted using the Laser Doppler Velocimetry (LDV, Flow Explorer 2D-Dantec), a method valued for its non-intrusive nature and precision in velocity measurement through laser beams. This technique operates when a particle scatters laser light upon crossing the intersection of two laser beams, with the scattered light collected by a receiving lens. The accuracy of the measurements provided by the manufacturer, for a range of 0–10 m.s⁻¹, is ±0.012 m.s⁻¹. To enable LDV measurements, smoke particles were introduced into the air stream using a smoke generator, with particle velocity measured at various points inside the trays.

For the purpose of this experiment, the original carton airtight clamshells (ACs) were substituted with ACs made from polymethyl methacrylate (PMMA). This alteration was made to enable LDV measurements through the transparent walls of the ACs while maintaining the same dimensions as the original carton variants. The measurements were done at the mid-height of the ACs in the positions indicated in Fig. 3a. Only component in the main airflow direction (V_x) was measured. Two repetitions were carried out, and the maximum standard deviation obtained was 0.02 m.s⁻¹.

3. Mathematical model

A 3D model of strawberries multi-packaging system was developed, with the computational domain divided into three subdomains: the free

airflow fluid zone, the solid tray zone, and the AC zones. Only half of the trays were modelled, relying on the assumption of symmetry within the packaging system (as shown in Fig. 4), which served to reduce the computational time required for the simulations.

The modelling approach did not involve the direct representation of strawberries within the ACs. Instead, the interior of the ACs was simulated as a solid block with equivalent thermal characteristics. In a first approach, the following formula was used to calculate the equivalent thermal conductivity of the medium inside an AC (Urquiola et al., 2017):

$$\lambda_{eq} = \lambda_s^{1-\epsilon} \lambda_a^\epsilon \tag{1}$$

where ϵ is the porosity.

The equivalent thermal characteristics of the solid block consider the overall air volume in the AC. However, this approach assumes that the solid block is homogeneous, the air is uniformly distributed in the AC, and heat transfer occurs solely by conduction. Therefore, the presence of a separate air layer above the solid block, commonly observed within clamshells (both ventilated and non-ventilated), does not globally alter the characteristics of the equivalent solid medium. Instead, it contributes to more easily generating local natural convection in the area defined by the air layer and increasing the thermal conductivity of the equivalent medium.

By applying Eq. (1), we obtained a value of 0.08 W.m⁻¹.K⁻¹. However, this equation neglects the effect of natural convection inside the AC. Using the height of the AC (95 mm) as the characteristic dimension and considering a temperature differential of 16 °C (between the cooling air and the AC at the beginning of precooling), the Grashof number was determined to be 1.6 × 10⁶. This calculation underscores the need to account for natural convection inside the AC if the wall temperature of the AC is supposed close to the cooling air temperature.

In a preliminary experiment, using the same experimental setup described in Section 2.1, one AC within the tray was chosen and filled with the PVC strawberries, while the remaining ACs were left empty. Seven strawberries within the selected AC were instrumented with thermocouples to follow their temperatures during cooling under a specified airflow rate, adhering to the same experimental protocol. The experiments were conducted for two different AC positions. After each experiment, the average HCT of the seven monitored strawberries was calculated.

A preliminary CFD model was developed, treating the interior of the selected AC as a solid block, while the other ACs remained empty. The

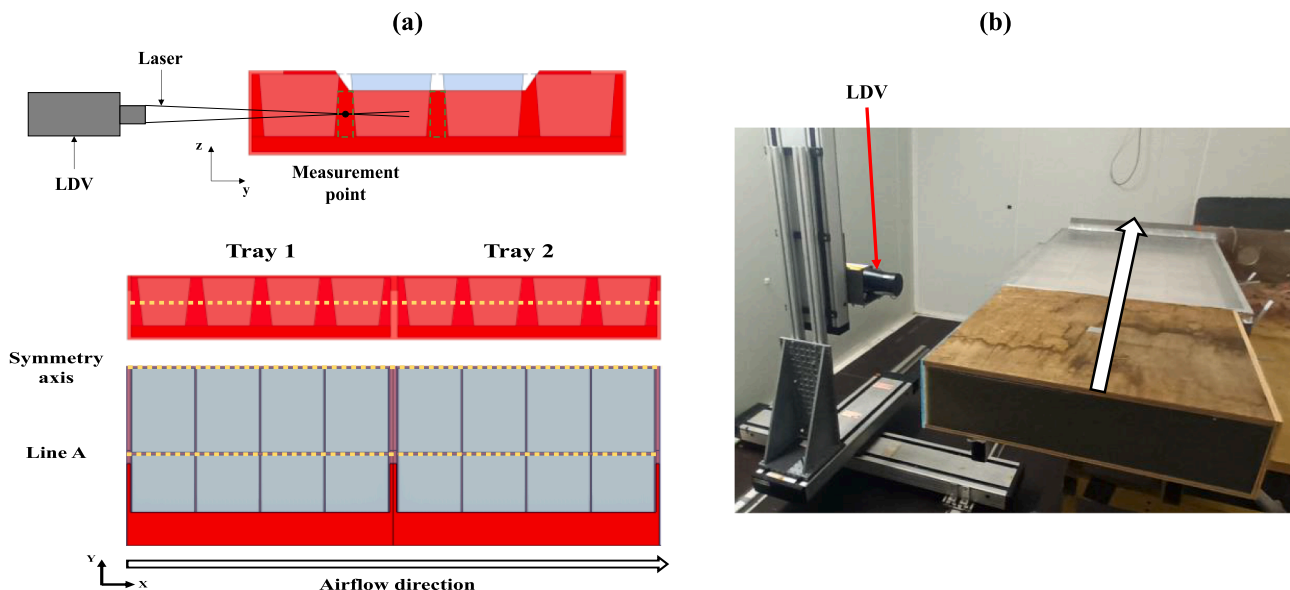


Fig. 3. (a) LDV measurement positions, (b) LDV with the experimental device.

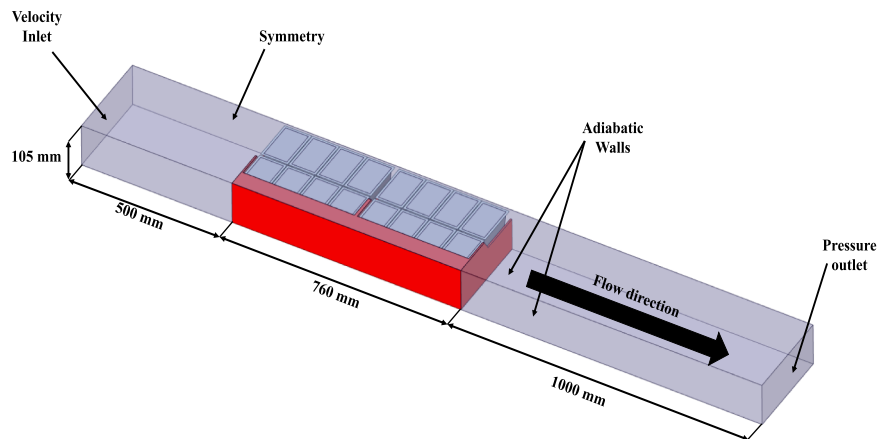


Fig. 4. CFD model.

model simulated both the airflow and the heat transfer, including conduction and convection.

Using the model, a sensitivity analysis was carried out to find the suitable λ_{eq} for the solid block taking into account the potential effect of natural convection of the heat transfer. A value of $0.12 \text{ W.m}^{-1}.\text{K}^{-1}$ was found by minimizing the difference between the experimental and numerical HCT for the two positions. The difference between this value of $0.12 \text{ W.m}^{-1}.\text{K}^{-1}$ and $0.08 \text{ W.m}^{-1}.\text{K}^{-1}$ obtained from Eq. (1) reflects the effect of the natural convection of air embedded in the solid block.

The attributes of this equivalent solid block were defined as follows: $\rho_{eq} = 381 \text{ kg.m}^{-3}$; $\lambda_{eq} = 0.12 \text{ W.m}^{-1}.\text{K}^{-1}$; $C_{p,eq} = 4094 \text{ J.kg}^{-1}.\text{K}^{-1}$.

3.1. Boundary and operating conditions

In the computational model, the surfaces of the trays and ACs were treated as no-slip walls with no roughness. The side walls of the tray were assigned a heat flux of zero. Initially, the entire computational domain was set to a uniform temperature of $20 \text{ }^\circ\text{C}$ to simulate equilibrium with the ambient conditions. The inlet of the computational domain was characterised as a velocity inlet based on experimental measurements conducted using the LDV at the entrance of the experimental setup. Consequently, the airflow rate was established at 4.4 l s^{-1} , which is half of the experimentally recorded value. The exit of the computational domain was designated as a pressure outlet, where uniform atmospheric pressure was applied. The temperature at the domain's inlet was fixed at $4 \text{ }^\circ\text{C}$, representative of the refrigerated room's conditions. As our study focuses exclusively on heat transfer and the precooling stage of the cold chain, the respiration effect was considered negligible and was not considered in the simulations.

3.2. Numerical solution procedure

The turbulent flow was modelled using the Reynolds-Averaged Navier-Stokes (RANS) equations, with the $k-\epsilon$ turbulence model employing an Enhanced Wall Treatment function. The realizable $k-\epsilon$ model has proven to give good accuracy in simulations involving food packaging (Agyeman et al., 2023; O'Sullivan et al., 2016). In the simulations, buoyancy effects were deemed insignificant and thus excluded, indicating a reliance on forced-convection flow. The computational grid was generated with hybrid elements (tetrahedral and hexahedral cells) using the Fluent mesh generation software. The mesh ensured a maximum y^+ value of less than 5, which is appropriate for the turbulence model used. To ascertain the most accurate mesh setup, a mesh sensitivity analysis was undertaken. Different mesh sizes were evaluated, including 4.1×10^5 , 1.6×10^6 , 6.8×10^6 , 1.1×10^7 and 2.0×10^7 cells. These configurations were compared based on the average velocity at the middle orifice and the average temperature of all solid blocks,

calculated at the average SECT. The analysis revealed a marginal temperature difference of $0.02 \text{ }^\circ\text{C}$ and a velocity difference of just 0.02% between the 1.1×10^7 and 2.0×10^7 cell meshes. This indicates that increasing the number of grid cells beyond 1.1×10^7 does not significantly enhance the accuracy of the results. Moreover, such an increase would lead to a disproportionate rise in computational time, suggesting that a mesh size of 1.1×10^7 cells is optimal for balancing precision and computational efficiency. It is important to note that the high number of cells in this case was necessitated by the design of the AC edges, which created a minimum airspace of 2 mm between the ACs on the top side. To accurately capture the airflow diffusing from the headspace into the vertical channels between the ACs, a finer mesh was required in these regions.

The simulation was performed using ANSYS Fluent 21 software. The ‘‘Coupled’’ algorithm, combined with a second-order upwind technique, was utilized to solve the pressure-velocity-temperature coupled equations.

In order to lower the computational time, a steady-state simulation was performed first to resolve the momentum equations and to establish the flow field and the initial temperature conditions. After that, the flow and momentum equations were deactivated, and the transient simulation of the cooling process was run solving only the energy equation. The transient simulation operated with a time step of 120 s . The simulations took approximately 16 h (to simulate 22 h of cooling) on a computer with a 2.4 GHz Intel® Xeon® Silver 4210 R CPU and 256 GB of RAM.

4. Alternative design

In a previous study, Nasser eddine et al. (2023, 2024) underscored how adding ventholes to the actual tray design (TD 1) slightly enhanced the convective heat transfer coefficient (CHTC) on the AC walls and the cooling time. However, increasing the headspace above the ACs (from 5 mm to 28 mm) significantly decreased the CHTCs and increased the cooling time compared to TD 1. In light of these findings, we opted to use the developed model to better understand the airflow and cooling behaviours within TD 1 and to compare the performance of different tray designs (shown in Fig. 5). The focus will be on the influence of adding circular vent holes and their positions on the airflow behaviour and the cooling rate. The assessment was conducted under a consistent inlet airflow rate.

TD 2, which is comparable in size to TD 1 but includes four additional circular vent holes (each 30 mm in diameter) on the tray's longitudinal front face, was selected. Additionally, another alternative tray design (TD 5), which was not studied experimentally before in terms of CHTC and cooling time, was explored. This design shares the same dimensions as TD 2 and TD 1, but its three orifices are in front of the air pathways between the ACs within the tray. Note that TD 3 & 4, studied

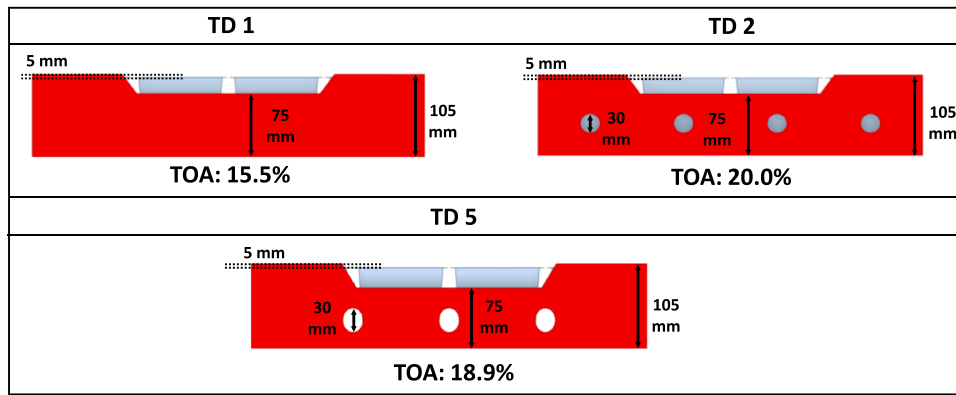


Fig. 5. Different tray designs (TAO: total opening area percentage).

in Nasser eddine et al. (2024, 2023) do not appear in this manuscript. The name "TD 5" was used to avoid confusion between the two papers.

5. Results and discussion

5.1. Experimental validation

5.1.1. Airflow validation

Fig. 6 presents a comparison between the simulated and measured air velocities (x-component velocity, V_x) and fluctuating velocities (Root mean square velocity, V_{RMS}) in the pathways between the ACs within the tray, specifically at the tray's mid-height along the symmetry axis and line A (Fig. 3), for TD 1 (each red marker reflects the average of two repetitions).

Numerical fluctuating velocity was calculated using the familiar Boussinesq relationship (Versteeg and Malalasekera, 1995):

$$-\rho \overline{v_i v_j} = \mu_t \left(\frac{\partial v_i}{\partial x_j} + \frac{\partial v_j}{\partial x_i} \right) - \frac{2}{3} \rho k \delta_{ij} \quad (2)$$

Where v' ($\text{m}\cdot\text{s}^{-1}$) is the fluctuating velocity represented by V_{RMS} in Fig. 6, μ_t ($\text{kg}\cdot\text{m}^{-1}\cdot\text{s}^{-1}$) is the turbulent viscosity, k ($\text{m}^2\cdot\text{s}^{-2}$) is the turbulent kinetic energy, ρ ($\text{kg}\cdot\text{m}^{-3}$) is the air density and V ($\text{m}\cdot\text{s}^{-1}$) is the mean velocity.

The results demonstrate that the model accurately predicts the overall trend of airflow related to V_x and V_{RMS} . However, the model overestimates the velocities along the central pathway (symmetry axis). The velocity in the central channel is notably twice as high as that in Line A, which can be attributed to the central channel's direct alignment with the main trapezoidal orifice. As can be seen, the longitudinal velocity experiences a gradual increase in the main flow direction between the inlet and outlet tray sections. This increase reflects dynamic exchange with the upper airflow in the thin headspace leading to jet deviation downwards (Fig. 9) and thus to an increase of air velocities in the lower part.

Higher V_{RMS} can be noticed at the tray inlet at the symmetry plane (Fig. 6) due to the divergent effect of the jet flow, including jet deviation next to the inlet section which enhances the turbulence by increasing velocity gradients. On the contrary, the lowest V_{RMS} values observed at the tray exit reflect the convergent effect of this section, which tends to laminarise the flow and thus reduce the turbulence.

On the other hand, the overall good agreement between the model and experiments related to air velocity helps to gain confidence in the numerical predicted heat transfer coefficients at AC walls as they are directly driven by air velocities.

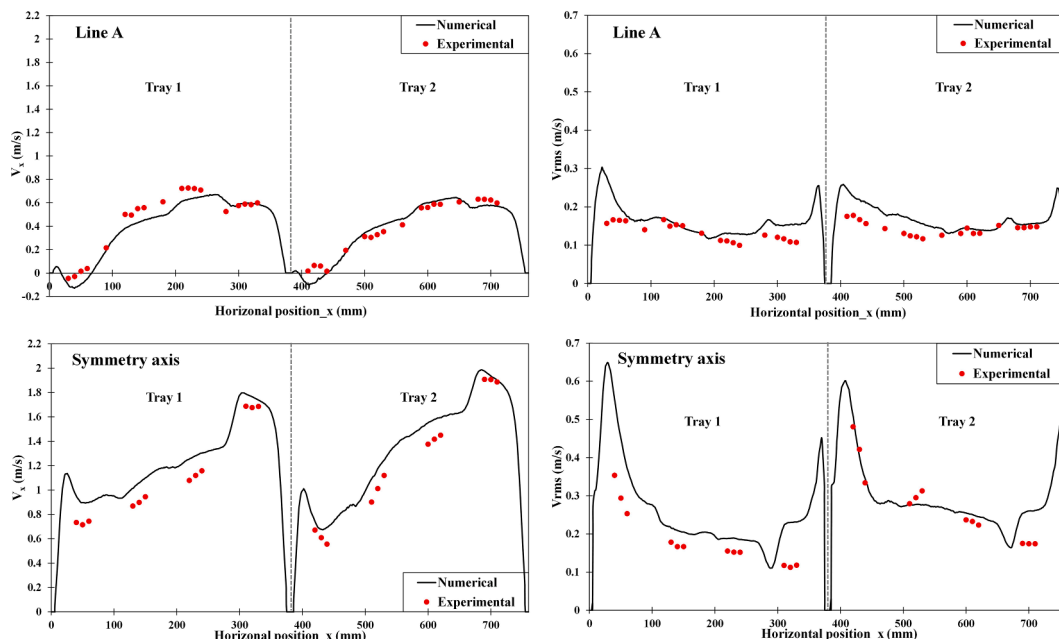


Fig. 6. Comparison of measured and numerical velocities (V_x and V_{RMS}) for TD 1 along line A and symmetry axis.

5.1.2. Thermal validation

Fig. 7 displays a comparison between the experimental HCT and SECT with the respective predicted values from the numerical model. For the experimental results, the HCT and SECT are calculated as the mean values from the five instrumented strawberries in each designated position. On the numerical side, the average HCT and SECT are derived from five specific points within the solid block that align with the center of gravity coordinates of the instrumented PVC strawberries.

Overall, the model predicted well the cooling rate with RMSE values of 0.42 h and 0.81 h for the HCT and SECT, respectively. In both experimental and numerical results, the shorter cooling times are for AC1 and AC9, located at the air inlets of tray 1 and 2, respectively, while the longer cooling times correspond to AC8 and AC16, located at the exit corner of each tray. The comparison of average cooling kinetics for each tray, as depicted in Fig. 8, between the values predicted by the model and those measured experimentally shows that the model generally captures the cooling behaviour.

5.2. Airflow behaviour

Fig. 9 displays the airflow dynamics within two trays for the tray design TD 1, where air enters via the main trapezoidal opening and speeds up as the flow area narrows. Subsequently, the airflow splits into distinct streams, with the first stream passing through the headspace above the ACs. This type of jet flow issuing the main trapezoidal orifice behaves as a confined jet flow as explained by Agyeman et al. (2023).

The tray's enclosed space implies the development of a confined wall jet, maintaining its airflow rate constant due to the absence of lateral

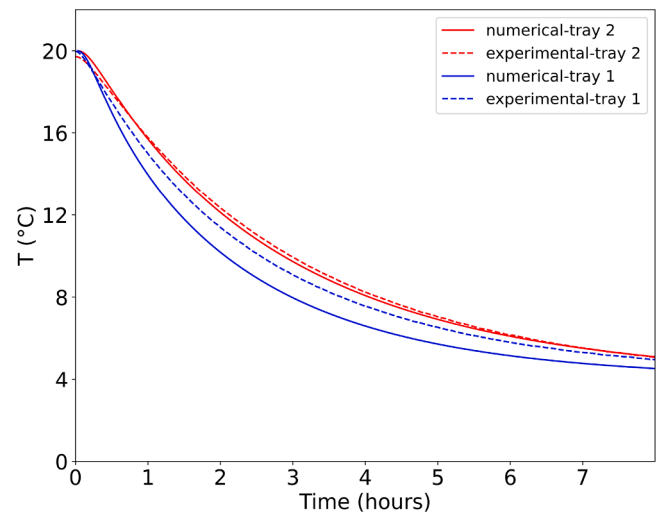


Fig. 8. Comparison between the average experimental cooling kinetics and the numerical ones for the ACs in each tray.

vent holes and, thus, to the lack of ambient air entrainment from the cold room. This confinement effect limits the jet's lateral diffusion (along the y-axis), entraining the development of a channel flow rather than a free-wall jet flow. The resulting airflow gives rise to a strong heterogeneity in the lateral direction. This heterogeneity is more pronounced near the tray's edges leading to the formation of an elongated recirculating cell

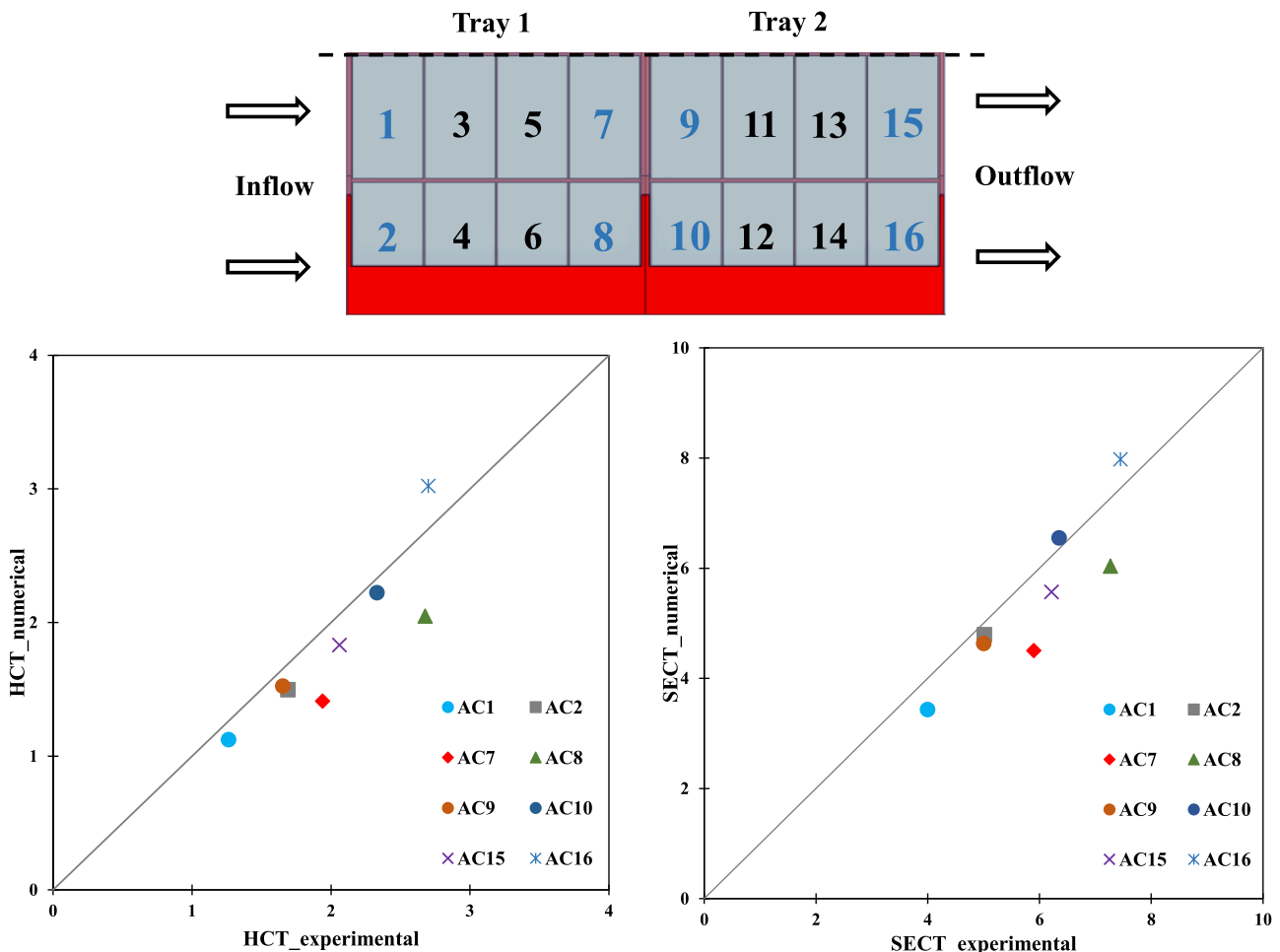


Fig. 7. Comparison of the average HCT (h) and SECT (h) obtained from the experimental data and from the numerical model for TD 1.

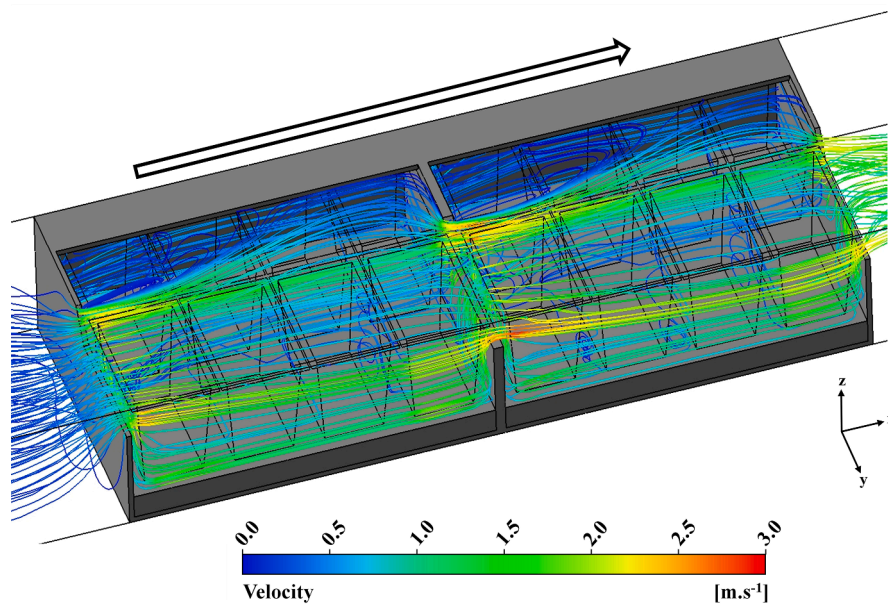


Fig. 9. Airflow streamlines patterns for TD 1.

with low velocities in the headspace and poor ventilation within the border channel (Fig. 10).

The lateral ventilation between the ACs along the y-axis is induced by the interaction of air fluxes flowing in the different pathways and the headspace. This ventilation appears to be weak when compared to longitudinal ventilation through different air pathways. This results in lower convective heat transfer coefficients on the ACs' walls facing these areas as identified by Nasser eddine et al. (2023). These lateral air pathways zones also exhibit air recirculation, due to interaction with vertical airflow originating from the headspace. The examination of the numerical data reveals the same airflow behaviour between the two trays.

In order to compare different tray designs, Table 2 displays the airflow percentages through the three pathways along the x-axis (Central pathway, pathway 1, and pathway 2 in Fig. 11) and in the headspace

above the ACs for the first and second trays.

It can be observed that the vent holes and their position affect the quantitative repartition of air fluxes between different zones of the trays. The introduction of vent holes in TD 2, positioned in front of the AC walls, enhances the ventilation of the pathways near the tray's edges, with airflow increasing from 13 % to 18 % and 10 % to 16 % for C (tray 1) and F (tray 2) respectively. Conversely, in TD 5, where vent holes are placed in front of the air channels, a preference for short-circuit airflow is observed, reducing ventilation of the zones at the edge of the tray. A notable reduction is seen in Tray 2 for pathway 2 (F section), where only 1 % of the airflow passes through. Due to its more balanced air fluxes between headspace and pathways, TD 2 enables a substantial reduction in pressure loss when compared to TD 1. From an additional simulation, it was observed that maintaining the same pressure difference as TD 1 (11.9 Pa) allowed 39 % more airflow for TD 2 (12.3 l s^{-1}).

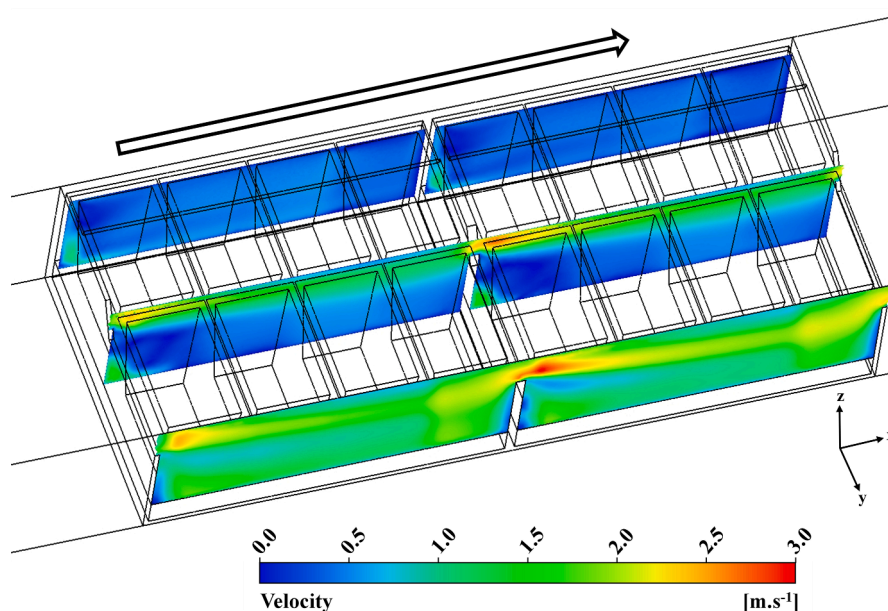


Fig. 10. Velocity contours of different vertical planes passing by the channels along the x-axis for tray design TD 1.

Table 2

Percentage of the airflow passing through the different pathways between the ACs and through the headspace above the ACs for the different tray design.

Design	Δp (Pa)	Q (l/s)	A	B	C	Tray 1 Headspace	D	E	F	Tray 2 Headspace
TD 1	11.9	4.4	36 %	27 %	13 %	24 %	36 %	28 %	10 %	26 %
TD 2	7.9	4.4	31 %	29 %	18 %	21 %	30 %	33 %	16 %	21 %
TD 5	6.4	4.4	32 %	45 %	5 %	19 %	34 %	48 %	1 %	17 %

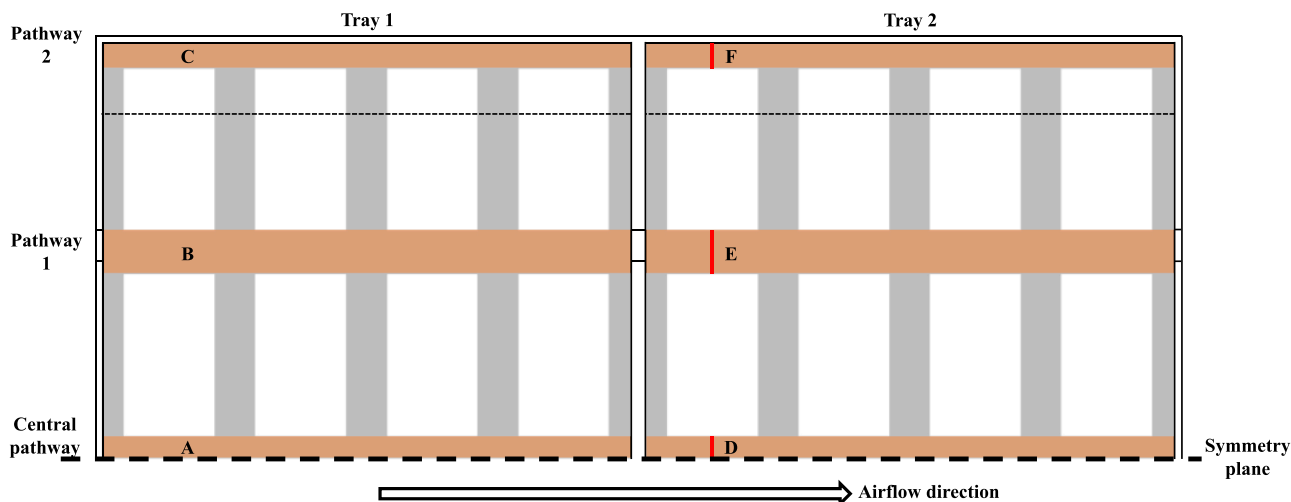


Fig. 11. Positions of the vertical plane in the pathways (A–F).

The airflow patterns in the headspace vary with each design (Fig. 12), notably at the tray edges. With the airflow in TD 2 and TD 5 being directed more through the channels between the ACs, the rate of airflow in the headspaces decreases. This reduction in the airflow rate leads to lower velocity in this area (headspace), mitigating the entrainment responsible for recirculation at the tray edges, a phenomenon clearly observable in TD 1. This impacts, of course, temperature distribution, as observed in Fig. 12.

5.3. Cooling behaviour

The airflow pattern discussed previously plays a crucial role in affecting the cooling rate and the heterogeneities within the system. As depicted in Fig. 13, after 2 h of cooling, there is a noticeable variation in temperature, ranging from 4 °C (air temperature in the pathways, blue colour) to 17.5 °C (temperature of the solid block within AC14 and AC13, red colour). A consistent rise in both air and product temperatures is observed along the airflow direction. This trend is more pronounced at the edge of the tray, where ventilation is poor.

Additionally, there is an evident temperature heterogeneity across the width of the tray, influenced by the described airflow dynamics. Specifically, the ACs positioned at the center of the trays (ACs 1,3,5,7,9,11,13, and 15) experience more effective ventilation compared to those at the edge (ACs 2,4,6,8,10,12,14, and 16). This temperature heterogeneity is particularly pronounced in the second tray, where the impact of the ventilation and the warmer air through the pathways at the tray’s edge becomes more significant.

The design of the tray substantially influences airflow behaviour, which in turn affects cooling efficiency. Fig. 14 features cartographies illustrating how different tray designs impact characteristic cooling times (average HCT of the solid bloc).

TD 2 shows improvement in both the homogeneity and the rate of cooling of ACs, especially those positioned in front of the orifices. For instance, in AC2, the HCT is reduced from 1.43 h to 1.07 h, and in AC10, the HCT decreases from 2.23 h to 1.67 h. Conversely, tray design TD 5, where vent holes induce a preferential airflow short-circuit, leads to

increased cooling heterogeneity and extends the rate of the cooling of the ACs, particularly those at the edge of the tray due to the reduced ventilation as demonstrated in Table 2. The effect of that is more pronounced when observing AC 8 and AC 16, where the HCT increased respectively from 1.90 h for TD 1 to 2.43 h for TD 5 and from 2.67 h to 3.30 h.

6. Conclusion

A CFD model was developed to analyse heat transfer and airflow within a pallet of strawberries packed in airtight clamshells during air-forced precooling. Focusing on a half layer of the pallet, the model treated the contents of the clamshells, both air and strawberries, as an equivalent solid block. The comparison of experimental data with the model’s predictions showed a good agreement, affirming the model’s validity.

Analysis of the airflow within the actual tray design TD 1 revealed the presence of two distinct regions: a well-ventilated central zone and a poorly ventilated area at the edge of the tray. This uneven airflow significantly impacted the cooling efficiency of the products inside the clamshells, resulting in two distinctive cooling trends — along the airflow direction and across the tray’s width.

For Modified Atmosphere Packaging (MAP), integrating edges to the clamshell to seal the film influences airflow patterns. These edges act as quasi-barrier, separating the airflow ventilating the AC top wall from the airflow around the vertical walls. This emphasizes the importance of selecting the proper headspace height, which emerges as the most critical factor for achieving equal airflow distribution between the headspace and the vertical walls.

Additional vent holes in the tray, when optimally positioned, could promote more balanced airflow between the pathways, enhancing cooling uniformity and efficiency while reducing overall pressure loss.

The validated numerical model could serve as a design tool for optimising future packaging configurations. It enables systematic exploration of various design modifications, such as:

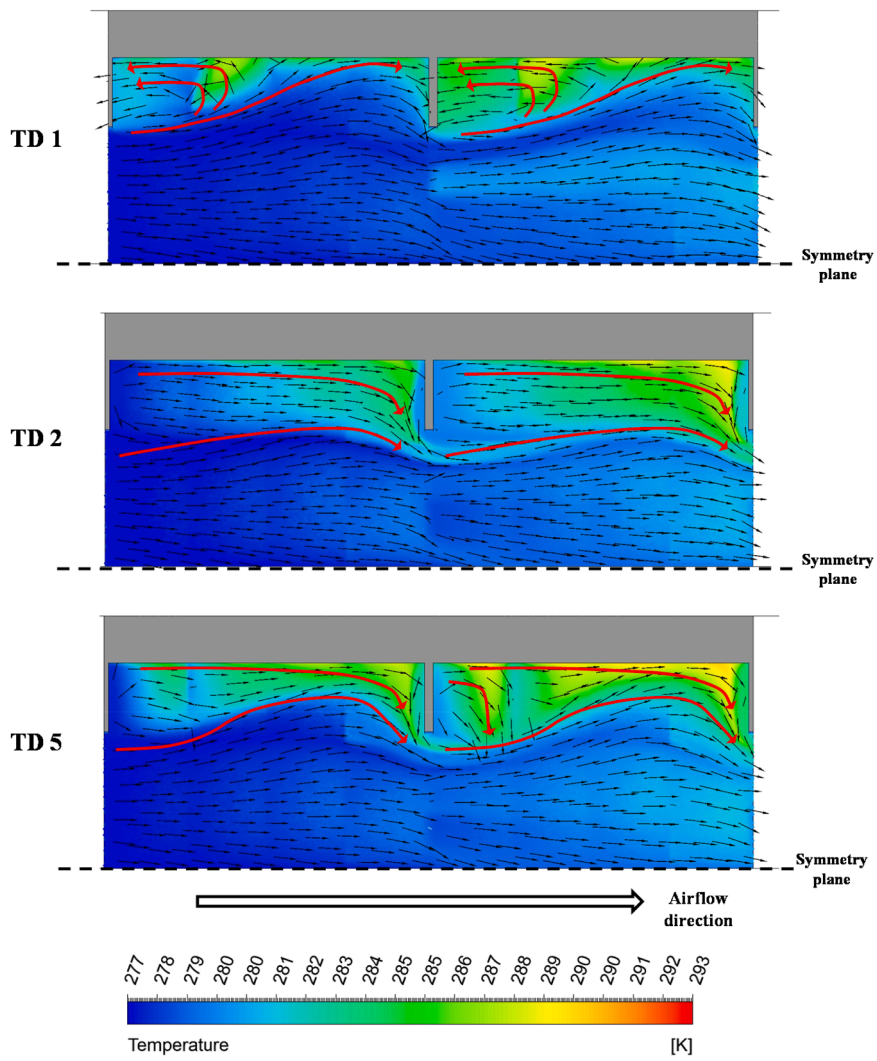


Fig. 12. Velocity vectors and temperature contour at a plane passing in the headspaces after 2 h of cooling.

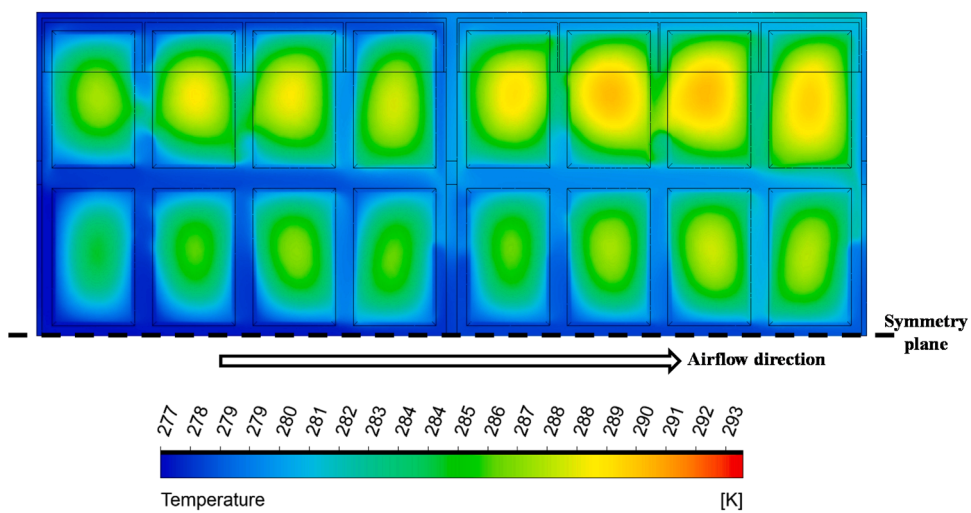


Fig. 13. Temperature contour at the mid-height of the ACs after 2 h of cooling for TD 1.

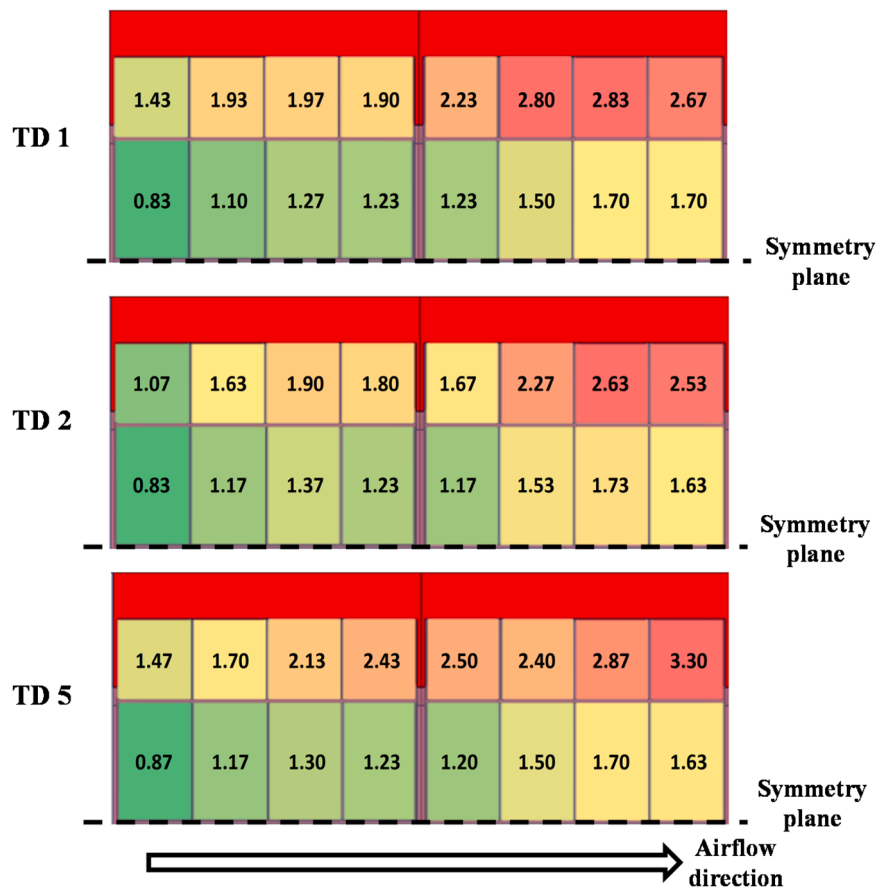


Fig. 14. Average HCT (h) at each AC position for different tray designs: TD 1, TD 2, and TD 5.

- 1- Adjusting the dimensions of trapezoidal vent holes to enhance the ventilation of the regions at the edge of the tray.
- 2- Evaluating mesh-like packaging design, akin to plastic bins, to improve cooling performance.
- 3- Analysing the impact of clamshell sealing edges, such as evaluating a design that mimics plastic clamshells without edges but operates under modified atmosphere conditions.

However, selecting the optimal configuration among the different designs requires an integrated assessment that goes beyond ventilation and cooling parameters. This assessment should also consider mechanical performance, cost, logistical factors (packaging's ability to integrate smoothly and efficiently into the entire cold chain), and environmental impact.

CRediT authorship contribution statement

Ahmad Nasser eddine: Writing – original draft, Visualization, Validation, Methodology, Investigation, Formal analysis, Data curation, Conceptualization. **Steven Duret:** Writing – review & editing, Supervision, Conceptualization. **Denis Flick:** Writing – review & editing, Supervision, Conceptualization. **Jean Moureh:** Writing – review & editing, Supervision, Conceptualization.

Declaration of competing interest

The authors declare that they have no known competing financial interests or personal relationships that could have appeared to influence the work reported in this paper.

Acknowledgments

The authors thank the French National Research Agency for the opportunity and financial support to carry out this project, under project EcoFreshChain, ANR-20-CE21-0007.

References

- Agyeman, E.K.K., Duret, S., Flick, D., Laguerre, O., Moureh, J., 2023. Computational modelling of airflow and heat transfer during cooling of stacked tomatoes: optimal crate design. *Energies* 16 (4). <https://doi.org/10.3390/en16042048> (Basel).
- Alvarez, G., Flick, D., 1999a. Analysis of heterogeneous cooling of agricultural products inside bins Part I: aerodynamic study. *J. Food Eng.* 39 (3), 227–237. [https://doi.org/10.1016/S0260-8774\(98\)00164-2](https://doi.org/10.1016/S0260-8774(98)00164-2).
- Alvarez, G., Flick, D., 1999b. Analysis of heterogeneous cooling of agricultural products inside bins Part II: thermal study. *J. Food Eng.* 39 (3), 239–245. [https://doi.org/10.1016/S0260-8774\(98\)00166-6](https://doi.org/10.1016/S0260-8774(98)00166-6).
- Ambaw, A., Fadiji, T., Opara, U.L., 2021. Thermo-mechanical analysis in the fresh fruit cold chain: a review on recent advances. *Foods* 10 (6). <https://doi.org/10.3390/foods10061357>.
- Anderson, B.A., Sarkar, A., Thompson, J.F., Singh, R.P., 2004. Commercial-scale forced-air cooling of packaged strawberries. *Trans. ASAE* 47 (1), 183–190. <https://doi.org/10.13031/2013.15846>.
- Berry, T.M., Umezuruike Linus Opara, Mulugeta Admasu, Delele., 2015. Geometric Design Characterisation of Ventilated Multi-scale Packaging Used in the South African Pome Fruit Industry. *Agric. Mech. Asia Afr. Lat. Am.* 46 (3). https://posth.arvestinnovation.org.za/wp-content/uploads/2015/09/AMA46_3-Sum_Tarl-Berry.pdf.
- Dehghannya, J., Ngadi, M., Vigneault, C., 2010. Mathematical modeling procedures for airflow, heat and mass transfer during forced convection cooling of produce: a review. *Food Eng. Rev.* 2 (4), 227–243. <https://doi.org/10.1007/s12393-010-9027-z>.
- Dehghannya, J., Ngadi, M., Vigneault, C., 2011. Mathematical modeling of airflow and heat transfer during forced convection cooling of produce considering various package vent areas. *Food Control* 22 (8), 1393–1399. <https://doi.org/10.1016/j.foodcont.2011.02.019>.
- Delele, M.A., Ngcobo, M.E.K., Getahun, S.T., Chen, L., Mellmann, J., Opara, U.L., 2013a. Studying airflow and heat transfer characteristics of a horticultural produce

- packaging system using a 3-D CFD model. Part I: model development and validation. *Postharvest Biol. Technol.* 86, 536–545. <https://doi.org/10.1016/j.postharvbio.2013.08.014>.
- Delele, M.A., Ngcobo, M.E.K., Getahun, S.T., Chen, L., Mellmann, J., Opara, U.L., 2013b. Studying airflow and heat transfer characteristics of a horticultural produce packaging system using a 3-D CFD model. Part II: effect of package design. *Postharvest Biol. Technol.* 86, 546–555. <https://doi.org/10.1016/j.postharvbio.2013.08.015>.
- Duret, S., Hoang, H.M., Flick, D., Laguerre, O., 2014. Experimental characterization of airflow, heat and mass transfer in a cold room filled with food products. *Int. J. Refrig. Rev. Int. Froid* 46, 17–25. <https://doi.org/10.1016/j.ijrefrig.2014.07.008>.
- Ferrua, M.J., Singh, R.P., 2009. Modeling the forced-air cooling process of fresh strawberry packages, Part I: numerical model. *Int. J. Refrig.* 32 (2), 335–348. <https://doi.org/10.1016/j.ijrefrig.2008.04.010>.
- Gruyters, W., Defraeye, T., Verboven, P., Berry, T., Ambaw, A., Opara, U.L., Nicolai, B., 2019. Reusable boxes for a beneficial apple cold chain: a precooling analysis. *Int. J. Refrig.* 106, 338–349. <https://doi.org/10.1016/j.ijrefrig.2019.07.003>.
- Hoang, H.M., Duret, S., Flick, D., Laguerre, O., 2015. Preliminary study of airflow and heat transfer in a cold room filled with apple pallets: comparison between two modelling approaches and experimental results. *Appl. Therm. Eng.* 76, 367–381. <https://doi.org/10.1016/j.applthermaleng.2014.11.012>.
- Mukama, M., Ambaw, A., Opara, U.L., 2020. Advances in design and performance evaluation of fresh fruit ventilated distribution packaging: a review. *Food Packag. Shelf Life* 24. <https://doi.org/10.1016/j.fpsl.2020.100472>.
- Nalbanti, H., Seiedlou, S., 2020. Sensitivity analysis of the precooling process of strawberry: effect of package designing parameters and the moisture loss. *Food Sci. Nutr.* 8 (5), 2458–2471. <https://doi.org/10.1002/fsn3.1536>.
- Nasser eddine, A., Duret, S., Flick, D., Laguerre, O., Sdiri, I., Moureh, J., 2024. Heat transfer within a multi-package: assessing the impact of package design on the cooling of strawberries. *J. Food Eng.* 382. <https://doi.org/10.1016/j.jfoodeng.2024.112190>.
- Nasser eddine, A., Duret, S., Flick, D., Moureh, J., 2023. Convective heat transfer characteristics within a multi-package during precooling. *J. Food Eng.* 359. <https://doi.org/10.1016/j.jfoodeng.2023.111710>.
- Nasser Eddine, A., Duret, S., Moureh, J., 2022. Interactions between package design, airflow, heat and mass transfer, and logistics in cold chain facilities for horticultural products. *Energies* 15 (22). <https://doi.org/10.3390/en15228659> (Basel).
- Ngcobo, M.E.K., Delele, M.A., Opara, U.L., Meyer, C.J., 2013. Performance of multi-packaging for table grapes based on airflow, cooling rates and fruit quality. *J. Food Eng.* 116 (2), 613–621. <https://doi.org/10.1016/j.jfoodeng.2012.12.044>.
- O'Sullivan, J., Ferrua, M.J., Love, R., Verboven, P., Nicolai, B., East, A., 2016. Modelling the forced-air cooling mechanisms and performance of polylined horticultural produce. *Postharvest Biol. Technol.* 120, 23–35. <https://doi.org/10.1016/j.postharvbio.2016.05.008>.
- Pathare, P.B., Opara, U.L., Vigneault, C., Delele, M.A., Al-Said, F.A.J., 2012. Design of packaging vents for cooling fresh horticultural produce. *Food Bioprocess Technol.* 5 (6), 2031–2045. <https://doi.org/10.1007/s11947-012-0883-9>.
- Pham, A.T., Moureh, J., Flick, D., 2019a. Experimental characterization of airflow within a pallet of product generating heat: application for cheese product. *Int. J. Refrig.* 106, 89–103. <https://doi.org/10.1016/j.ijrefrig.2019.06.022>.
- Pham, A.T., Moureh, J., Flick, D., 2019b. Experimental characterization of heat transfer within a pallet of product generating heat. *J. Food Eng.* 247, 115–125. <https://doi.org/10.1016/j.jfoodeng.2018.12.003>.
- Urquiola, A., Alvarez, G., Flick, D., 2017. Frost formation modeling during the storage of frozen vegetables exposed to temperature fluctuations. *J. Food Eng.* 214, 16–28. <https://doi.org/10.1016/j.jfoodeng.2017.06.025>.
- Versteeg, H.K., Malalasekera, W., 1995. *An Introduction to Computational Fluid Dynamics: the Finite Volume Method*. Longman Scientific & Technical, Essex, England.
- Wang, D., Lai, Y., Jia, B., Chen, R., Hui, X., 2020. The optimal design and energy consumption analysis of forced air pre-cooling packaging system. *Appl. Therm. Eng.* 165. <https://doi.org/10.1016/j.applthermaleng.2019.114592>.
- Wang, D., Lai, Y.H., Zhao, H.X., Jia, B.G., Wang, Q., Yang, X.Z., 2019. Numerical and experimental investigation on forced-air cooling of commercial packaged strawberries. *Int. J. Food Eng.* 15 (7). <https://doi.org/10.1515/ijfe-2018-0384ARTN20180384>.
- Wu, W., Haller, P., Cronje, P., Defraeye, T., 2018. Full-scale experiments in forced-air precoolers for citrus fruit: impact of packaging design and fruit size on cooling rate and heterogeneity. *Biosyst. Eng.* 169, 115–125. <https://doi.org/10.1016/j.biosystemseng.2018.02.003>.
- Zhao, C.J., Han, J.W., Yang, X.T., Qian, J.P., Fan, B.L., 2016. A review of computational fluid dynamics for forced-air cooling process. *Appl. Energy* 168, 314–331. <https://doi.org/10.1016/j.apenergy.2016.01.101>.